Journal of Fluorescence, Vol. 8, No. 4, 1998

Lanthanide Luminescence as a Probe of Nanocrystalline Materials

Brian M. Tissue[1,3] and Bipin Bihari[1,2]

Received January 25, 1998; accepted May 8, 1998

The sharp lines in the optical spectra of lanthanide ions in solids are sensitive to the local environment surrounding the ion and, therefore, provide a local probe to study new materials. This paper reports the laser spectroscopic characterization of a series of Eu_2O_3 nanocrystals, which serve as a model compound for understanding the spectroscopy of lanthanides in nanocrystalline materials. The optical spectra of Eu_2O_3 particles with diameters of approximately 18 to 4 nm show an increase in inhomogeneous broadening and a transition to a very disordered phase as the particle size decreases. The $^5D_0$ fluorescence transients of the nanocrystals are shorter than in bulk material show no clear trend as a function of particle size but do become single exponential for 6- and 4-nm particles.

KEY WORDS: Lanthanide fluorescence; nanocrystals; phosphors; Eu_2O_3; monoclinic structure; laser spectroscopy.

INTRODUCTION

Nanophase and nanocrystalline materials are polycrystalline solids with particle diameters of 100 nm or less. The large surface-to-volume ratio of nanometer-size particles determines the structure and chemistry of the particles, which in turn controls the structural, electronic, and optical properties of the materials. Nanocrystals can form in new phases [1] or exhibit enhanced structural, electronic, and optical properties [2–4]. They therefore offer new possibilities for advanced phosphor applications. The development of new types of flat-panel and projection displays has created a need for optical phosphors with new or enhanced properties [5]. Nanocrystalline materials also provide model compounds for using fluorescence spectroscopy to study the surface structure and interparticle chemistry at interior surfaces in bulk polycrystalline materials.

Lanthanide-doped cubic-phase Y_2O_3 and related materials are common phosphors in optical display and lighting applications [6], and the search for new phosphors has led to the preparation of nanocrystalline forms of Y_2O_3 [7–10]. Gas-phase condensation of nanocrystalline Eu_2O_3 and Y_2O_3 of approximately 20-nm diameter results in the formation of the monoclinic crystal structure [8,11,12], rather than the usual cubic structure [13]. Eu_2O_3 through Dy_2O_3 in the lanthanide series can form in the monoclinic structure at high temperature or high pressure [13–15], but Y_2O_3 and lanthanide sesquioxides with a smaller ionic radius than Dy_2O_3 require both high temperature and high pressure [14]. Formation of nanocrystalline Y_2O_3 in this denser metastable phase at ambient conditions has been attributed to an additional hydrostatic pressure component, resulting from the Gibbs–Thomson effect [11].

The monoclinic phase of these sesquioxides has space group C2/m, and the lattice possesses three crystallographically distinct cation sites, each having point

[1] Department of Chemistry, Virginia Polytechnic Institute and State University, Blacksburg, Virginia 24061-0212.
[2] Present address: Mail Code K9900, University of Texas—Austin, 10100 Burnet Road, Building 160, Austin, Texas 78758.
[3] To whom correspondence should be addressed.

1053-0509/98/1200-0289$15.00/0

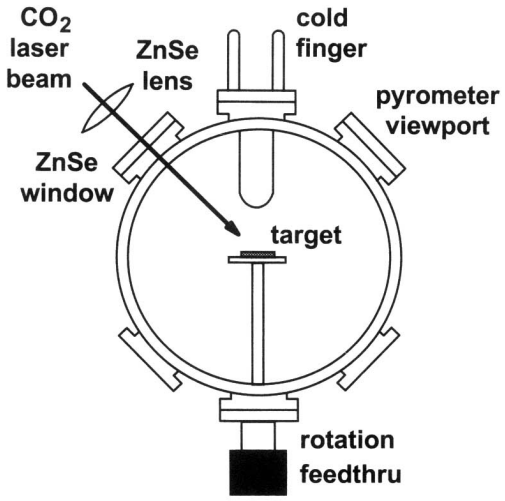

Fig. 1. Schematic of the nanocrystal preparation chamber.

Table I. Effect of Chamber Pressure on the Resulting Size of Eu_2O_3 Nanocrystals

Chamber pressure (Torr)	Average particle diameter (nm)	Crystal structure
400	18	Monoclinic
100	12	Monoclinic
10	6	Transitional
1	4	Cubic (disordered)

group symmetry C_s [16,18]. All three cation sites are sevenfold coordinated. The coordination of two cation sites (Ln I and Ln II) can be described by six oxygens at the apices of a trigonal prism with a seventh oxygen lying along the normal to a face. The coordination of the third site (Ln III) is described as a distorted octahedron with a seventh oxygen at a long distance (3.13 Å for Eu_2O_3) [14,16–18]. Optical spectroscopic studies of bulk monoclinic Eu_2O_3 [15,19], Eu^{3+}:Gd_2O_3 [18,20], and Eu^{3+}:Y_2O_3 [21] show that the Eu^{3+} ion occupies the three nonequivalent crystallographic sites in the monoclinic structure, producing three distinct sets of optical spectra. Theoretical energy-level splittings for the ^7F_j energy levels were generated from ab initio calculation of the crystal-field parameters for each cation site in monoclinic Eu^{3+}:Gd_2O_3 [18]. These calculations indicated that the three distinct sets of optical spectra, labeled sites A, B, and C, correspond to cation sites Ln III, Ln II, and Ln I, respectively.

Preliminary work showed that the optical spectra of nanocrystal Eu_2O_3 larger than approximately 10 nm have the same overall energy-level splitting pattern for the three cation sites as in the bulk monoclinic Eu_2O_3 [7]. However, the spectral lines of the nanocrystals were broadened, and a "secondary phase" increases in dominance as the particle diameter becomes smaller. This paper reports the optical spectroscopy of Eu_2O_3 nanocrystals as a function of particle size. The goals of the experiments are to determine the utility of using lanthanide fluorescence as a probe to understand the structure and defect chemistry of nanocrystalline materials and to investigate the optical properties of fluorescent dopant ions in confined geometries.

EXPERIMENTAL

A bulk Eu_2O_3 sample was prepared by heating a pressed pellet at 1400°C for 4 h and letting it cool at the intrinsic rate of the furnace. Nanocrystalline samples of Eu_2O_3 were prepared by a gas-phase condensation technique [7,8,12]. Figure 1 shows a schematic of the preparation chamber. A CO_2 laser heats a spot on a ceramic target consisting of a pressed and sintered pellet of Eu_2O_3. The laser power was typically 40 W and vaporize material that forms gas-phase clusters. The target temperature was monitored with an optical pyrometer and was typically 2500°C. The nanocrystalline particles collected on the cold finger, which was filled with 50–60°C water to keep the quenching temperature constant. Vaporization took place in a nitrogen atmosphere at different pressures, and Table I summarizes the Eu_2O_3 nanocrystal size dependence as a function of chamber pressure. Most particles for a given preparation condition were approximately ±25% of the average diameter based on a survey of electron micrographs. The phase and particle sizes of the nanocrystalline material were characterized by transmission electron microscopy (TEM) and powder X-ray diffraction (XRD). The particle sizes were determined from X-ray diffraction linewidths using the Scherrer equation [22] and from a survey of the TEM micrographs. The assignment of the crystal structures is described with the spectral results discussed below.

For optical spectroscopy, the materials were packed into a depression on a copper sample holder, which was mounted on the cold head of a closed-cycle refrigerator (Cryomech GB 15). All of the spectra were recorded at a sample temperature of approximately 13 K to eliminate thermally populated energy levels and broadening of the transitions. All spectra and decay transients were recorded using a Nd^{3+}:YAG-pumped dye laser with Coumarin 540A dye as the excitation source. Excitation

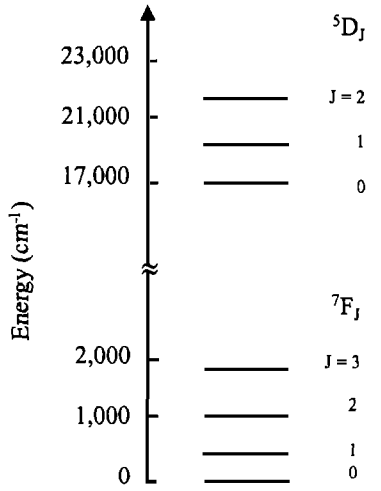

Fig. 2. Partial energy-level diagram of the Eu^{3+} ion in solids. Each level can be split into 2J+1 sublevels.

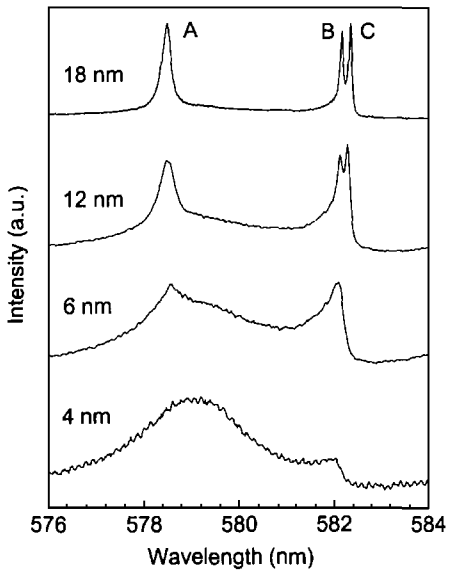

Fig. 3. $^7F_0 \rightarrow {}^5D_0$ excitation spectra of nanocrystalline Eu_2O_3. The spectra were recorded with the 0.25-m monochromator at 624 nm and a boxcar gate width of 150 μs. The *y*-axis for all spectra in this paper is fluorescence intensity in arbitrary units.

spectra were recorded by scanning the laser and monitoring fluorescence with a 0.25-m monochromator (6-nm bandpass) with a Hammamatsu P-28 photomultiplier tube (PMT). Fluorescence spectra were recorded by tuning the laser to an excitation line, and scanning a 1-m monochromator (Spex 1000M) that was equipped with a cooled GaAs PMT (Hammamatsu R-636). The PMT signal was processed with a boxcar averager (Stanford SR250), and stored using an analog-to-digital data-acquisition board (National Instruments Lab-PC+) and LabView computer program. Fluorescence transients were recorded with a 350-MHz digital oscilloscope (Tektronix TDS460) after typically averaging 200 laser shots.

OPTICAL SPECTRA

Figure 2 shows a simplified energy-level diagram of the Eu^{3+} ion in a solid host. The overall energy-level structure of the Eu^{3+} ion does not change in different hosts due to the shielding of the 4*f* electrons by outer shell 5*s* and 5*p* electrons [23]. Each energy level shown in Fig. 2 can be split into 2J + 1 sublevels. This fine structure is sensitive to the local crystalline field surrounding the Eu^{3+} ion, producing distinct spectra for each different crystallographic site that Eu^{3+} ions occupy. These fingerprint spectra makes Eu^{3+} an effective probe ion of the local structure. The spectra in this paper follow the site A, B, and C labeling notation for the monoclinic structure used in references [18,19].

Figure 3 shows the $^7F_0 \rightarrow {}^5D_0$ excitation spectra of the Eu_2O_3 nanocrystals. For the 18- and 12-nm samples, there are three distinct lines at 578.5, 582.1, and 582.3 nm, corresponding to sites A, B, and C, respectively. The spectrum of the 18-nm nanocrystals was essentially the same as bulk material, but with an increase in the inhomogeneous broadening. Figure 4 shows the $^7F_0 \rightarrow {}^5D_1$ excitation spectra of the Eu_2O_3 nanocrystals. As in Fig. 3, the spectrum of the 18-nm nanocrystals was essentially the same as bulk material. The labels at the top of the figure indicate the sharp lines in the spectra that correspond to sites A, B, and C. Figure 5 shows the $^5D_0 \rightarrow {}^7F_2$ fluorescence spectra for these samples. Energy transfer is rapid in this pure europium system, and exciting any of the sites results in fluorescence from the B and C sites, which are thermalized at 13 K.

The excitation spectra of the Eu_2O_3 nanocrystals in Figs. 3 and 4 show extensive broadening of the sharp site A, B, and C lines as the particle size decreases. In Fig. 3, a weak broad feature at 579 nm increases in intensity as the particle size decreases (this broad band is visible in the 18-nm sample when the *y* scale is expanded). Similar changes occur in the excitation and fluorescence spectra in Figs. 4 and 5. These broad lines are completely absent in bulk monoclinic Eu_2O_3 and are attributed to a "phase" transition as the particle size of the nanocrystals decreases. The broadened lines that dominate the 4-nm sample are attributed to a return to the regular cubic phase, although with a large amount

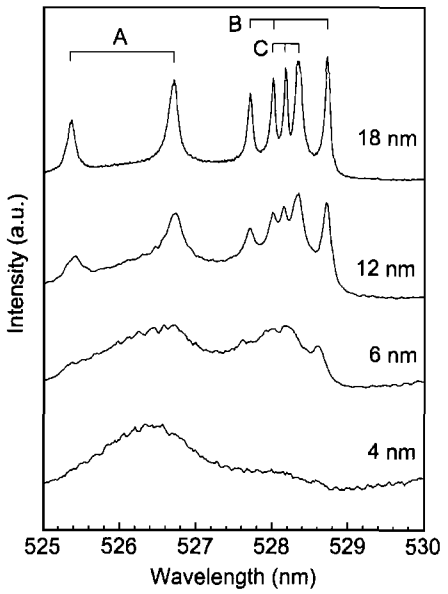

Fig. 4. $^7F_0 \rightarrow {}^5D_1$ excitation spectra of nanocrystalline Eu_2O_3. The spectra were recorded with the 0.25-m monochromator at 624 nm and a boxcar gate width of 150 μs.

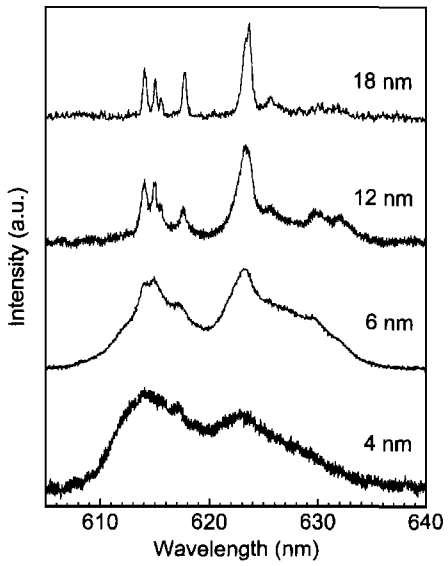

Fig. 5. $^5D_0 \rightarrow {}^7F_2$ fluorescence spectra of nanocrystalline Eu_2O_3 exciting the $^5D_0$ level at approximately 578.5 nm and with a boxcar gate width of 150 μs.

of disorder. Powder XRD patterns and annealing experiments are consistent with this interpretation [24].

FLUORESCENCE DYNAMICS

The $^5D_0$ fluorescence transients of Eu_2O_3 are nonsingle exponential, but can be approximated with a biexponential fit. No fluorescence is observed from the $^5D_1$ level in either the bulk or the nanocrystalline Eu_2O_3. Table II lists the results of least-squares fits to the $^5D_0$ fluorescence transients of bulk and nanocrystalline Eu_2O_3. The decay time of the 18-nm sample is shorter than the decay time of the bulk material. Reduced quantum efficiency and lifetime as phosphor particle size decreases have been attributed to quenching by surface defects [6]. No clear trend is observed in the $^5D_0$ fluorescence transients of the Eu_2O_3 nanocrystals as a function of particle size. An unexplained lengthening of the fluorescence transient occurs when the Eu_2O_3 particle diameter decreases from 18 to 12 nm. The fluorescence transients of the 6- and 4-nm samples fit well to a single-exponential function. This change to single-exponential decay is attributed to the disappearance of a distribution of cross-relaxation rates since the small particle diameter eliminates the distribution of distances between the Eu ions.

Table II. $^5D_0$ Fluorescence Decay Times of Eu_2O_3 Nanocrystals: The Dual Numbers Are for a Biexponential Fit

Average particle diameter	$^5D_0$ decay time (μs)
Bulk (>1 μm)	12/61
18 nm	8/36
12 nm	25/250
6 nm	40
4 nm	38

Figure 6 shows extended scans of the excitation spectra of the 12-, 6-, and 4-nm Eu_2O_3 particles. A large increase in the intensity of hot bands compared to the normal excitation lines occurs as the particle size decreases. There is no line broadening and no observation of hot bands in the fluorescence spectra that would indicate that the sample is at an elevated temperature. The increase in hot-band intensity in Fig. 6 suggests that the smaller particles have a nonequilibrium storage of population in the $^7F_1$ level and, presumably, also in other low-lying excited states. This result suggests that there is a decrease in the population of optical phonons that facilitate nonradiative relaxation, which is counter to predictions that the density of states of high-energy phonons will increase as size-specific resonances become possible in the smaller particle sizes [25]. Recent high-resolution homogeneous linewidth measurements on Eu_2O_3 and Eu^{3+}:Y_2O_3 nanocrystals show an exponential temperature dependence, which is attributed to a Raman-scattering dephasing mechanism [26]. The exponential term arises due to the size-restricted nature of the pho-

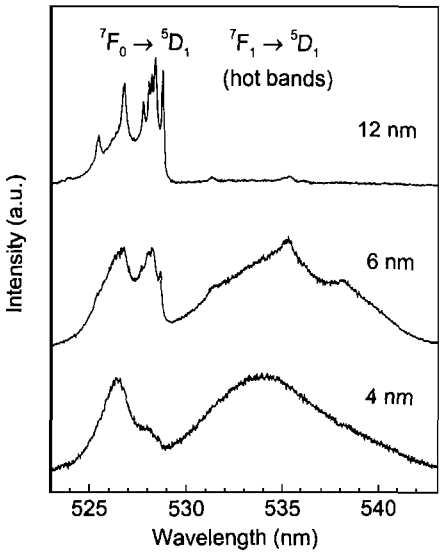

Fig. 6. Excitation spectra of nanocrystalline Eu_2O_3 showing the $^7F_1 \rightarrow {}^5D_1$ hotband region. The spectra were recorded with the 0.25-m monochromator at 624 nm and a boxcar gate width of 150 μs.

non density of states. Simulations can reproduce the temperature dependence of the linewidths, however, the simulations do not match the particle-size dependence. The data suggests that there is a phonon limit that corresponds to a larger size than the actual physical particle size. One explanation is that the phonon limit arises from propagation of phonons between particles that are in contact. A possible hypothesis to explain the increase in hot-band intensity and these other results is that the electron–phonon coupling of the Eu^{3+} ions is different for surface and bulk phonons.

SUMMARY

The optical spectra of 18-nm Eu_2O_3 particles confirm the powder XRD results that the nanocrystals form in the monoclinic crystal structure. The optical spectra also show an increase in the inhomogeneous broadening compared to the spectra of bulk Eu_2O_3 and the presence of broad features due to a second phase. The broad bands increase in intensity as the particle size decreases and completely dominate the spectra of 4-nm Eu_2O_3 particles. The broad lines of the 4-nm particles are attributed to cubic-phase Eu_2O_3, although with extensive disorder.

This phase transition from the monoclinic phase to a highly disordered cubic phase for the smallest particles suggests that the more open cubic structure can better accommodate the inherent disorder of the surfaces and provides a lower surface energy. Obviously some other factor(s) besides the Gibbs–Thomson effect controls the overall crystal structure at very small particle sizes. The structure of the 6-nm particles is described as transitional, because the XRD patterns and optical spectra contain features of both the monoclinic and cubic phases. Determining whether this dual character results from the distribution of particle sizes or due to a true transitional crystal structure will require further work.

The spectral results in this paper show that the Eu^{3+} ion provides an excellent probe of the local structure of metal–oxide nanocrystals and provides a basis to use Eu^{3+} spectroscopy to investigate nanocrystals as a function of annealing and surface modification. The fluorescence dynamics results remain puzzling and will require further experiments to obtain a clear picture of the phonon dynamics and electron–phonon coupling in these materials.

ACKNOWLEDGMENTS

This work was supported by the National Science Foundation (CAREER award CHE-9502460) and by a Research Corporation Cottrell Scholars Award.

REFERENCES

1. Z. Li, H. Hahn, and R. W. Siegel (1988) *Mater. Lett.* **6**, 342.
2. R. P. Andres *et al.* (1989) *J. Mater. Res.* **4**, 704.
3. G. C. Hadjipanayis and R. W. Siegel, Eds. (1993) *Nanophase Materials: Synthesis–Properties–Applications*, NATO ASI Series E **260**, Kluwer, Dordrecht.
4. H. Gleiter (1989) *Prog. Mater. Sci.* **33**, 223.
5. P. Maestro and D. Huguenin, (1995) *J. Alloys Comp.* **225**, 520.
6. T. Hase, T. Kano, E. Nakazawa, and H. Yamamoto (1990) *Adv. Electron. Electron Phys.* **79**, 271.
7. H. Eilers and B. M. Tissue (1996) *Chem. Phys. Lett.* **251**, 74.
8. B. Bihari, H. Eilers, and B. M. Tissue (1997) *J. Luminesc.* **75**, 1.
9. E. T. Goldburt *et al.* (1997) *J. Luminesc.* **72–74**, 190.
10. Y. Tao *et al.* (1996) *Mater. Lett.* **28**, 137.
11. G. Skandan *et al.* (1992) *Nanostruct. Mater.* **1**, 313.
12. H. Eilers and B. M. Tissue (1995) *Mater. Lett.* **24**, 261.
13. L. Eyring, (1979) in K. A. Gschneidner, Jr., and L. Eyring (Eds.), *Handbook on the Physics and Chemistry of Rare Earths, Vol. 3*, North-Holland, Amsterdam, p. 337.
14. H. R. Hoekstra (1966) *Inorg. Chem.* **5**, 754.
15. G. Chen, N. A. Stump, R. G. Haire, and J. R. Peterson, (1992) *J. Alloys Comp.* **181**, 503.
16. H. T. Hintzen and H. M. van Noort (1988) *J. Phys. Chem. Solids* **49**, 873.
17. H. L. Yakel, (1979) *Acta Cryst.* **B35**, 564.
18. J. Dexpert-Ghys, M. Faucher, and P. Caro (1981) *Phys. Rev. B* **23**, 607.
19. K. C. Sheng and G. M. Korenowski, (1988) *J. Phys. Chem.* **92**, 50.
20. D. Rice and L. de Shazer, (1970) *J. Chem. Phys.* **52**, 172.

21. D. K. Williams, B. Bihari, B. M. Tissue, and J. M. McHale (1998) *J. Phys. Chem. B* **102**, 916.
22. J. Doss and R. Zallen (1993) *Phys. Rev. B* **48**, 15626, and references therein.
23. G. H. Dieke (1968) *Spectra and Energy Levels of Rare Earth Ions in Crystals*, Interscience, New York.
24. J. C. Milora and B. M. Tissue, unpublished results.
25. D. Wolf, J. Wang, S. R. Phillpot, and H. Gleiter (1995) *Phys. Rev. Lett.* **74**, 4686.
26. K. S. Hong, R. S. Meltzer, B. Bihari, D. K. Williams, and B. M. Tissue (1998) *J. Luminesc.* **76–77**, 234.